

Time Division Multiplexing Front-Ends for Multiantenna Integrated Wireless Receivers

Gautham Krishnamurthy, *Student Member, IEEE*, and Kevin G. Gard, *Member, IEEE*

Abstract—The approach of time division multiplexing (TDM) within an integrated wireless receiver to reduce the power, area and cost of multiple antenna receivers is studied. A solution is proposed to address the cross-interference between multiplex channels that affected previous attempts at TDM for multiple receive antennas. Detailed analysis from a radio system viewpoint is provided for when TDM is used as a low complexity hardware technique for managing multiple antenna channels. Simple closed form noise figure relations in terms of the number of multiplex channels and the anti-alias filter rejection are developed. Noise figure expressions that relate an individual TDM amplifier or TDM amplifier array's noise figure to that of a regular static amplifier are also given. These simple relations provide a quick method of determining expected noise figure of such systems. A four-antenna 2.4 GHz LNA array circuit in CMOS is designed in a 0.18- μm technology. The noise and linearity performance of this circuit is measured to verify the developed theory. The results obtained show close agreement with the developed model of the TDM-based multiantenna receiver system.

Index Terms—Amplifiers, array signal processing, diversity methods, multiple-input-multiple-output (MIMO), switched circuits, switching circuits, time division multiplexing (TDM).

I. INTRODUCTION

TRADITIONAL single antenna wireless communications receivers are hard pressed to provide improvements in system capacity and reliability demanded of present day cellular and broadband wireless systems. These challenges have led to the development and deployment of methods such as diversity [2], [3], adaptive beamforming [4], and multiple-input-multiple-output (MIMO) [5] to boost spectral efficiency of the communication link as well as improve system robustness. One characteristic common to all these methods is the use of multiple antennas at the transmitter and/or receiver, often under the umbrella of smart antenna technology [1]. Digital cellular technologies such as 3.5 and 4 G, and wireless networking technologies such as IEEE 802.11n/WLAN and 802.16e/WiMAX have adopted multiantenna techniques as an integral part of their standards. The other reasons for the use of multiple antennas in wireless transceivers are to support operation across disparate frequency bands and simultaneous multi-standard wireless operation. The commercial state-of-the-art [15], [16] in integrated antenna array wireless systems is the replication of receiver

Manuscript received January 12, 2009; revised May 06, 2009. This work was supported by the Analog Devices Raleigh Design Center, Raleigh, NC. This paper was recommended by Associate Editor A. Demosthenous.

The authors are with the Department of Electrical and Computer Engineering, North Carolina State University, Raleigh, NC 27695 USA (e-mail: gkrishn@ncsu.edu; kevin_gard@ncsu.edu).

Digital Object Identifier 10.1109/TCSI.2009.2031759

chains by brute force for each antenna element to leverage the advantages of sophisticated digital signal processing (DSP) at baseband. The duplication of receive circuits results in a linear increase in power consumption and cost in circuit area for each additional receive path included in the implementation. Signal combining at RF or IF following conventional phase shifting networks in the RF [17], IF or LO [18] signal paths is the other alternative. These combining approaches, although lowering the chip area and power to various degrees depending on the location of signal combining in the receive chain, are cumbersome to implement and control. They also result in the loss of spatial multiplexing (SM) gains provided by true MIMO. The loss in SM gains is because individual antenna information is no longer available following signal combining.

The twin trends of greater antenna diversity and availability of cheaper digital processing closer to the antenna in the receiver chain has created a need for low power, small silicon footprint hardware in the spirit of low cost CMOS integration. This has spurred the development of receiver circuits which support antenna diversity while keeping duplication of critical high power front-end circuits to the minimum. Many alternative receiver architectures are possible for accommodating antenna arrays and adaptive beamforming, which are becoming increasingly prevalent because of the numerous advantages they offer [1]–[5].

Due to the low cost and increasing integration possible with scaled CMOS technologies, one method that is highly attractive is the concept of antenna switching for time division multiplexing (TDM) onto a single receive channel. In this method, which has a long history [7]–[11], a reduction in RF hardware is obtained by switching individual elements of the antenna array onto a single RF channel. The switching is done at a high enough rate for the desired signal modulation at each antenna to be recoverable by digital processing at baseband.

The possible use of a rotating antenna switcher to sample antenna signals in a diversity reception system was proposed as early as 1931 by Beverage and Peterson [9] in their work that addresses the fading phenomenon in short wave radiotelegraphy. However, implementation of the switcher was not described in their work. There is, however, an acknowledgement of likely difficulty in achieving receiver selectivity due to the sidebands generated in such an antenna switching system. Interestingly it is very much the same reasons that has held back or led to the pursuing of a different approach [19] in recent history.

The formal theory of time division multiplexing was presented in a treatise by Bennett [7] in 1941. This classic work besides developing the general theory of time division multiplex systems, also discusses its implications on the bandwidth and crosstalk of these systems. Bennett's treatment also predicted that the restrictions on gain and phase characteristics would be

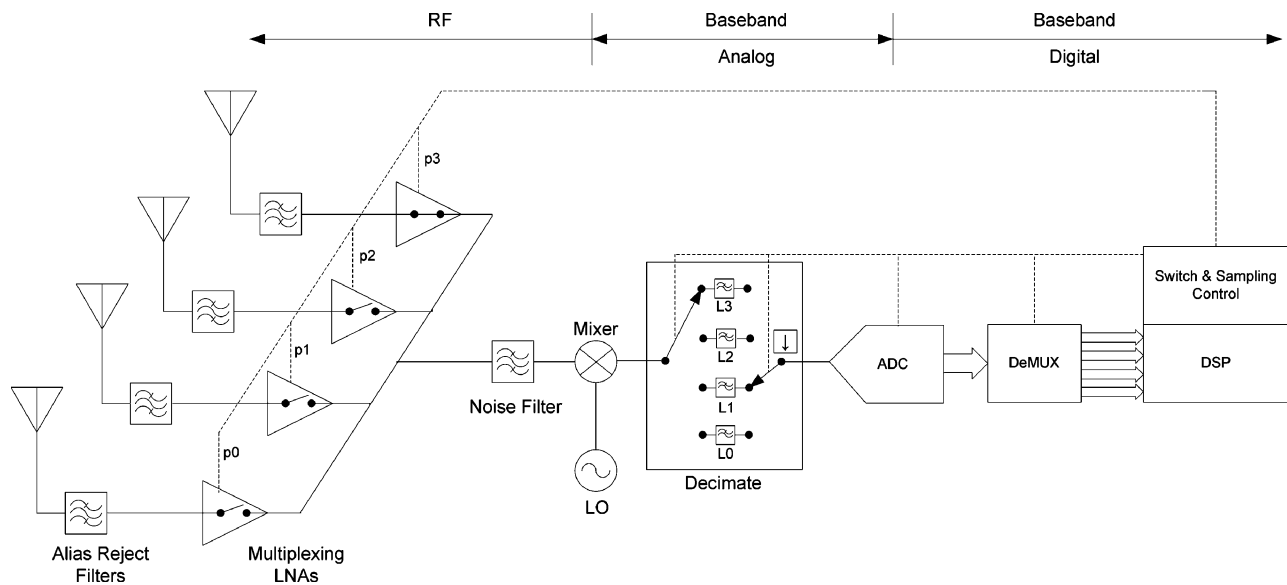


Fig. 1. TDM front-end multiantenna integrated receiver architecture.

stringent if economy of the bandwidth is desired in the multiplex systems. Some of the origins of what was formalized as the sampling theorem by Shannon in 1948 are clearly visible in this early work. A detailed historical account that traces the evolution of the TDM idea to the present day sampling theorem is available in [8]. Another paper on TDM important from an historic context is [12] that analyzes and offers closed form results for multiplex channel crosstalk.

The spatial multiplexing of local elements (SMILE) scheme for digital beamforming [13] is another recent avatar of the antenna switching idea. The SMILE work demonstrated a low-complexity proof of concept system for processing microwave phased array signals by multiplexing them in time. The prototypes developed showed experimental results for beamforming and direction of arrival estimation. They were implemented as antenna arrays incorporating discrete switching devices on a circuit board. The passive diode switches used in their initial work gave rise to problems with noise and speed of the array antenna system. The amplifying switching elements used later reduced these problems somewhat, but the problems associated with changing antenna loading due to the multiplexing action of the switches still remained [14]. Careful design of the array feed network therefore became necessary. Moreover the developed structures were bulky and not amenable to easy integration. The SMILE architecture as presented by Itoh *et al.* envisions the use of multiple channels with multiple analog-to-digital converters (ADCs) for IF/baseband processing.

In [19], a single pair of ADCs is used for a dual-antenna system by shifting the antenna signals to positive and negative frequencies of a complex spectrum. One major downside to this technique is that it is restricted to systems with two antennas only.

Another more recent work [20] proposes the combining of signals at the RF stage after spreading them with mutually orthogonal code sequences, like in the CDMA system of communications, following which a single receive chain can be utilized. As in the TDM case presented here, this system runs into

the challenge of having to contend with RF input signals that are inherently wideband. Hence unless the front-end code modulation is done at very high, carefully managed rates, it is expected to suffer difficult noise and interference aliasing problems. A consequence of using high code modulation rates to overcome these problems is the requirement of parallel non-digital de-spreading circuits prior to digitization. Compared to an equivalent TDM system, therefore, the required high switching rates could make the baseband circuitry larger, more complex and challenging to design. However, the additional baseband hardware could simplify timing synchronization issues compared to a TDM approach. Moreover, successful implementation of this signal combining scheme could lead to some bandwidth savings compared to techniques such as TDM.

As is evident from the previous discussion, there have been other publications in the past that have proposed TDM or TDM-type solutions to the multiple antenna problem. However, to the authors' knowledge this is the first detailed treatment from a radio hardware perspective of the application of TDM to the design of a multiantenna receiver front-end. Following the analysis, the integration of RF front-end circuitry for time division multiplexing in an RF CMOS process is demonstrated. It is designed to explore the performance of a low power, low cost, low complexity, high speed/bandwidth, integrated front-end for multiple antenna receivers. Since high speed multiplex switches are relatively straightforward to implement in CMOS processes, it adds to the time multiplexing scheme's appeal. CMOS circuits also provide the wide signal path bandwidths inherently required by time multiplexed signals. The time multiplexed architecture is compatible with existing and developing trends in integrated CMOS receiver design.

II. TDM FOR MULTIANTENNAS RECEIVER

A. System Overview

The system block architecture for a TDM multiantenna receiver is shown in Fig. 1. In the front-end, RF signals from an

N element antenna array are merged into a single RF signal path by high speed switches after the active (amplifying) devices that are incorporated following the antennas. The multiplexed signal is then downconverted to baseband or low-IF by a direct conversion or a low-IF downconversion mixer.

The hardware cost savings of this multiple antenna receiver architecture is significant. The number of mixers and ADCs are reduced by a factor of $N - 1$ for an N antenna receiver. The real advantage of the TDM architecture lies in the simplicity of hardware, and the possibility of time sharing hardware at both RF and baseband in contrast to the code modulation architecture [20]. Also this arrangement for multiple antenna RF receivers leverages the increased bandwidth available as a result of process technology scaling. With digital processing becoming cheaper and more powerful, this architecture would prove very attractive for antenna array systems because of the greater flexibility offered with minimal hardware overhead. The digital flexibility permits reuse of the same general receiver circuits in different antenna diversity applications such as spatial diversity, adaptive beamforming and MIMO-SM.

As a multiplexed receiver, only one switch of the array is active at a time. This may be in the form of selection diversity switching or periodically rotated switching—time division multiplexing—at high rates for maximal-ratio, equal-gain combining or MIMO-spatial multiplexing operation. The discussion in this paper is restricted to time division multiplexing which is significantly more challenging, and rewarding, than selection diversity switching. The rotating switch combines the multiple antenna signals sequentially in time, and then uses one signal path to downconvert and digitize the single multiplexed signal. The switch rate would usually be much higher than the information symbol rate at the antennas, yet significantly lower than the RF carrier frequency. The multiplexed signal path has to be wideband in order to ensure the multiplexed channels do not interfere with each other, i.e., information from one time slot smear into another time slot, much like the inter-symbol interference (ISI) encountered in digital communications. This implies that the multiplexed signal cannot be subjected to channel select filtering. This has been a major stumbling block that has prevented the implementation of the TDM scheme in prior work [19] on multiantenna receivers. The solution proposed in this work is to implement a baseband circuit that demultiplexes the downconverted signal, applies channel select filtering on the individual antenna channels and then remultiplexes them for digitization by a single ADC. This analog baseband circuit is functionally equivalent to a digital decimator, and is indicated as a decimator in Fig. 1. The emergence of discrete-time charge-domain signal processing solutions for alias reject filtering in digital radio architectures [21] allows for the possibility that such a decimator circuit can be devised and implemented on an integrated circuit. All sampling and resampling operations right from the front-end onwards (including multiplexing) would have to be under synchronous clock control. The degree of mismatch in synchronization between the multiplex and demultiplex stages due to imperfections in the switch control signal distribution is an important concern in this architecture. These imperfections include skew and jitter [22], whose effects become more prevalent at higher switching rates. But, the clock derived switch control signals

being within a single die are more easily managed compared to wireline or wireless TDM communication links.

B. TDM Receiver Theory

Natural sampling is the simplest of sampling processes involving switch gating of analog waveforms as opposed to impulse and flat-top (zero-order hold) sampling. Natural sampling may also be termed rectangular pulse sampling. This type of sampling is therefore well suited for RF signals as other types of sampling place more stringent requirements on the hardware. The only major difference is that conventionally the technique and analysis is applied to bandlimited baseband signals sampled at traditional Nyquist rates and above. In the multiplexing context, natural sampling will be done at rates significantly lower than the RF carrier frequency, i.e., the RF signal is bandpass sampled.

The basic requirement for recovering data from each of the antenna elements is given by the bandpass sampling theorem [1]. With a real-valued bandpass signal bandwidth of B centered at carrier frequency f_c , spectral aliasing considerations specify that each element of the array must be sampled at a rate f_s given by

$$\frac{2f_c + B}{q} \leq f_s \leq \frac{2f_c - B}{q - 1} \quad (1)$$

where q is an integer given by

$$1 \leq q \leq \left\lfloor \frac{f_c}{B} + \frac{1}{2} \right\rfloor. \quad (2)$$

Bandpass sampling considerations indicate that this frequency translation or aliasing action will demand that B essentially be the *entire receive bandwidth* as stipulated by the communications standard. Bandwidth B would ultimately be determined by the band rejection provided by the RF filter immediately after the antenna, as anything outside the passband has potential for folding into the desired signal band due to the multiplexing operation. The theoretical minimum sampling rate is a pathological case corresponding to integer band positioning of the bandpass signal. This minimum sampling rate condition is simply stated as

$$f_s \geq 2B. \quad (3)$$

If u as the oversampling factor above this minimum rate, f_s is rewritten as

$$f_s = 2uB. \quad (4)$$

Condition (3) is not sufficient in the choice of f_s as an arbitrary selection could lead to corruption of message signal spectrum by an undesired overlapping of aliases. The optimum f_s corresponds to the quadrature sampling case and is tied to f_c by

$$f_s = \frac{4}{2p + 1} f_c \quad (5)$$

where p is an integer. Under this additional condition the signal spectrum and its aliases are optimally spaced away from each other, easing downconversion and filtering requirements in the receive path. At this sample rate the phase difference between

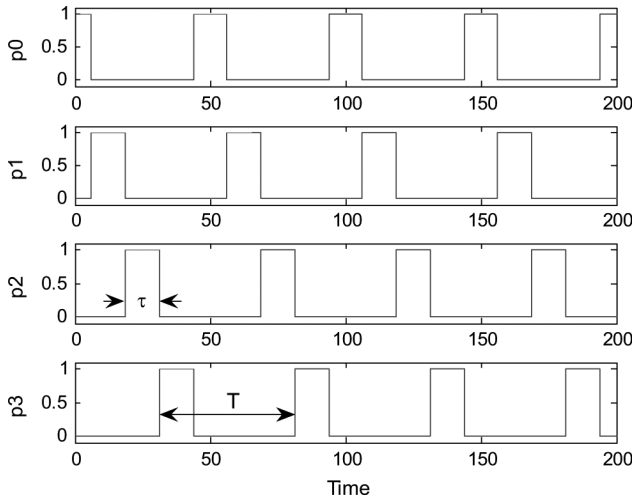


Fig. 2. LNA switch control pulses.

adjacent samples corresponds to $\pi/2$ at center frequency f_c implying that if the samples are sorted into odd and even sequences they may be processed in quadrature.

In the context of the multiplex system analysis, sample rate will refer to f_s , the pulse rate per antenna channel and multiplex rate to f_{mux} , the overall rate for all channels being multiplexed into a single RF stream. For the N element array, the multiplex rate will be

$$f_{\text{mux}} = Nf_s = 2uNB. \quad (6)$$

The switch control pulse train for time division multiplexing is shown in Fig. 2. The pulse interval is T corresponding to a frequency $f_s = 1/T$, and the pulse ‘‘ON’’ duration is $\tau = T/N$. The pulse train corresponding to the n th antenna channel may be expressed as

$$p_n(t) = \sum_{k=-\infty}^{\infty} \Pi\left(\frac{t - kT - n\tau}{\tau}\right) = \sum_{k=-\infty}^{\infty} \Pi\left(\frac{t - kT}{\tau} - n\right) \quad (7)$$

where $\Pi(t)$ is the rectangular function defined as

$$\Pi(t) = \begin{cases} 1, & \text{if } |t| < 0.5 \\ 0.5, & \text{if } |t| = 0.5 \\ 0, & \text{if } |t| > 0.5. \end{cases} \quad (8)$$

The Fourier transform of $p_n(t)$ is given by

$$\begin{aligned} P_n(f) &= \sum_{m=-\infty}^{\infty} P_m e^{-j2\pi m f_s n \tau} \delta(f - m f_s) \\ &= \sum_{m=-\infty}^{\infty} P_m e^{-j2\pi m n / N} \delta(f - m f_s) \end{aligned} \quad (9)$$

where P_m are the coefficients of the rectangular pulse train $p_0(t)$ in its Fourier series representation and is given by

$$P_m = \frac{\sin(m\pi f_s \tau)}{m\pi} = \frac{1}{N} \text{sinc}\left(\frac{m\pi}{N}\right). \quad (10)$$

The unnormalized sinc function is used in (10). The spectrum of the pulse train $p_0(t)$ is depicted in Fig. 3.

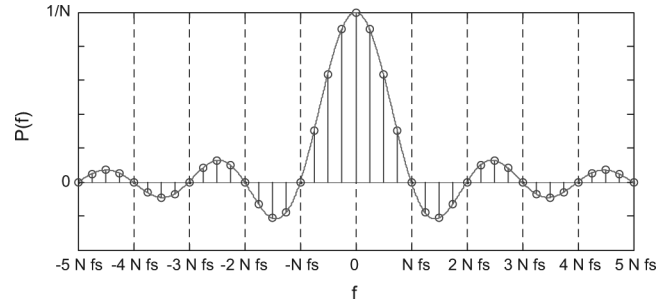


Fig. 3. Fourier series representation of rectangular pulse train.

Since ultimately individual antenna signals are of real importance for any meaningful baseband processing, it is their properties that need to be studied. It is also necessary to ensure that these individual signals are not unduly corrupted by any of the signal processing happening in the time shared receiver. On a per antenna channel basis, the result of the multiplexing operation is analogous to that of natural sampling, and may be expressed in equation form as

$$x_{ns}(t) = x_n(t) \cdot p_n(t) \quad (11)$$

where $x_n(t)$ is the time domain RF signal at the n th antenna. In frequency domain, this may be expressed as the following convolution operation:

$$\begin{aligned} X_{ns}(f) &= X_n(f) * P_n(f) \\ &= \sum_{m=-\infty}^{\infty} P_m e^{-j2\pi m n / N} X_n(f - m f_s) \end{aligned} \quad (12)$$

where $X_n(f)$ is the spectrum of the bandpass RF signal at the n th antenna.

Several important inferences may be drawn from (10) and (11), and Fig. 3.

- 1) If sections of the RF signal corresponding to each antenna channel are considered individually, replication of the original bandpass spectrum would be evident due to their sampled nature, the sampling being done with rectangular pulses. The spectral components repeat at intervals of f_s in the frequency domain and their envelope has the characteristic $\text{sinc}(x)$ shape.
- 2) The maximum power in the multiplexed signal spectrum is concentrated at f_c corresponding to the main tone ($m = 0$) of the pulse spectrum. The contribution of tones decrease as one moves away from the center of the pulse spectrum.
- 3) As $\tau \rightarrow 0$ or equivalently $N \rightarrow \infty$, pulse train becomes an impulse train and so does the pulse spectrum, spreading energy over all aliases in the multiplexed output equally while simultaneously reducing the signal power at each alias.
- 4) The zeroth replica ($m = 0$) power per antenna channel drops by $1/N^2$ as a result of the multiplexing action. This is often expressed as the pulse desensitization factor, the difference in magnitude of the peak pulse power and the main lobe power equal to $-20 \log(\text{duty cycle})$ or $20 \log(N)$ in dB scale. At the same time, the total signal power per antenna channel falls by $1/N$.

The RF signal spectrum per antenna channel is depicted in Fig. 4. The solid line shapes are aliases of the bandpass

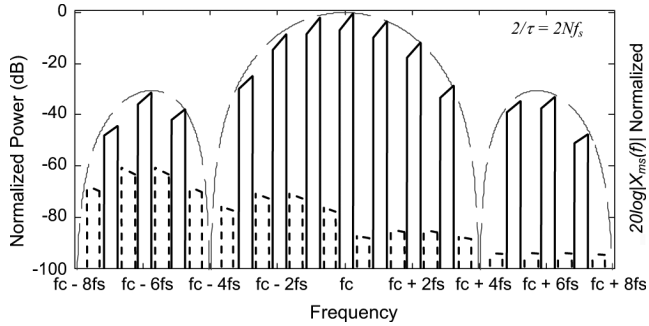


Fig. 4. Spectral components per antenna channel in TDM RF output.

content lying in the positive frequency region of the original (nonmultiplexed) spectrum and the dashed line shapes the negative frequency content that has aliased into the positive region. Quadrature processing would eliminate the negative (or positive) frequencies of the original spectra, thus offering the possibility of reduced f_s . This however comes with an area/power penalty.

The composite output from the multiplexer is simply a combination of the naturally sampled signals from the N antenna channels. The composite output of the multiplexer has spectral energy at multiples of f_s that should not be completely filtered out by any image reject filter following the LNAs. This is because any filtering to remove these spectral bands would lead to “cross-interference” between antenna channels that would make recovery of these channels impossible by simple demultiplexing at baseband [7], [12], [19]. The minimum theoretical bound for the number (W) of switching aliases around the center frequency to be passed in a TDM system to have the possibility of zero interchannel crosstalk is worked out by Bennett [7] to be

$$W \geq N \quad (13)$$

where N is the number of multiplexed channels. This bound is specified and valid for multiplex systems that employ impulse sampling. In practice the number of aliases required to minimize crosstalk would be more than N . The actual number of aliases allowed to pass through determines the multiplex signal bandwidth. In this context, since the noise (image-reject) filtering is eliminated or less stringent in direct conversion architecture or the low-IF architecture, these appear to be most suitable down-conversion schemes for the TDM receiver.

Mathematically the composite output may be written in the time domain as

$$x_{\text{mux}}(t) = \sum_{n=0}^{N-1} x_{ns}(t) = \sum_{n=0}^{N-1} x_n(t) \cdot p_n(t) \quad (14)$$

where $x_{\text{mux}}(t)$ is the multiplexed output and by using the linearity property of the Fourier transform, in the frequency domain as

$$\begin{aligned} X_{\text{mux}}(f) &= \sum_{n=0}^{N-1} X_{ns}(f) \\ &= \sum_{m=-\infty}^{\infty} P_n \sum_{n=0}^{N-1} e^{-j2\pi mn/N} X_n(f - mf_s) \end{aligned} \quad (15)$$

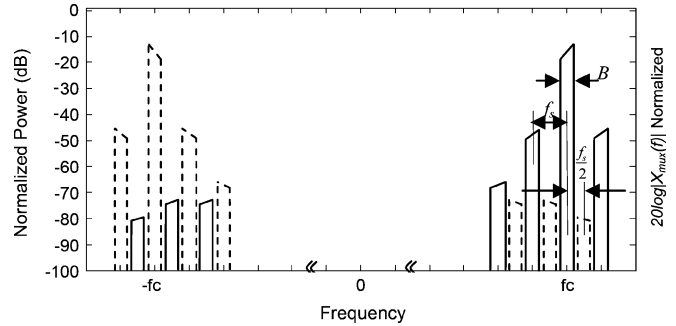


Fig. 5. Spectrum of TDM RF output.

where $X_{\text{mux}}(f)$ is the spectrum of the multiplexed output. Since the antenna signals are all bandpass filtered to occupy the same spectral band, chopping up and serializing these pulsed RF signals with the switching waveforms shown in Fig. 2 would result in a composite output that has the original frequency band’s spectral energy spread out over the harmonics of the switching function. In this respect the output from the LNA stage of the TDM receiver is *different* compared to that in a conventional single-path receiver. The output spectrum of the TDM front-end would appear as shown in Fig. 5.

Assuming a direct conversion scheme, the mixer would translate the entire composite signal spectrum of Fig. 5 down to baseband as in the conventional case. The multiplexed signal path cannot be subjected to channel select filtering due to cross-interference considerations. Hence, the multiplexed signal bandwidth would be too high for a single ADC to be able to handle. Therefore the signals will have to be decimated to lower rates if they are to be digitized by a single ADC. This decimation will require that each of the antenna channels be separated, i.e., demultiplexed in some form, before subjecting them to subband or channel select filtering. The rate change structure will slow the signal rates down to speeds that the ADC can handle.

The decimation, besides low pass filtering the demultiplexed signals, can include characteristics to reject the unwanted components at multiples of f_s . The filter cutoff frequency f_u should satisfy

$$\frac{B_{\text{sub}}}{2} < |f_u| < \frac{f_s}{d} - \frac{B_{\text{sub}}}{2} \quad (16)$$

where B_{sub} is the bandwidth of the desired wireless subband within the receive band of bandwidth B , and d is the downsampling factor in the decimation. Also,

$$B_{\text{sub}} \leq \frac{B}{d}. \quad (17)$$

The subband could contain one or more wireless channels, each of bandwidth B_{ch} .

The ADC sample rate may now be written as

$$f_{\text{ADC}} = \frac{f_{\text{mux}}}{d} = \frac{Nf_s}{d} = \frac{u}{d} N(2B). \quad (18)$$

Once digitized, the antenna signals may be subjected to additional channel select filtering to select channels of bandwidth B_{ch} before the enhanced multiantenna signal processing steps. The decimation structures’ and the ADC’s own spectral characteristic would be superimposed on the demultiplexed digital

data streams. Their spectral response envelope would contain factors of the form $\text{sinc}(ax)$, where a is a constant relative to the incoming sample rate. The final spectral shapes may be shaped by these sinc envelopes to provide nulls at predetermined frequencies to reject strong interferers.

C. Noise Analysis of TDM Receiver

The following noise sources are primarily relevant to noise analysis in a TDM system:

- (a) input thermal noise;
- (b) device added white noise;
- (c) phase noise (jitter) of switching clock.

In the noise analysis presented, only the wideband noise sources (a) and (b) that could be aliased inband are considered. Although it is expected that (a) and (b) noises will dominate, a more complete analysis should also take into consideration the impact of (c). The analysis of noise and SNR in the TDM case is very much like it is done for mixers, with the LO in the mixer being replaced by the switching clock pulses in this case. Mixers are generally analyzed as linear periodic time variant (LPTV) systems following the approach laid out in [23].

To allow a comparison TDM noise with a simpler case, the noise factor of a single amplifier of gain G is stated as

$$F_{\text{amp}} = \frac{\left(\frac{S}{N}\right)_{\text{in}}}{\left(\frac{S}{N}\right)_{\text{out}}} = \frac{1}{G} \frac{N_{\text{out,p}}}{N_{\text{inp}}} = 1 + \frac{N_a}{N_{\text{inp}}} = 1 + \frac{N_{ai}}{N_{\text{inp}}} \quad (19)$$

where

- $N_{\text{out,p}}$ available inband output noise power;
- N_{inp} available inband input noise power from the source;
- N_a added noise power from the amplifying device(s);
- N_{ai} input referred added noise power from the amplifying device(s).

The following general assumptions are made in the analyses that follow.

- 1) The gain G is wideband (over the multiplex signal bandwidth).
- 2) The available input noise $N_{in}(f)$ is white and stationary.
- 3) The bandpass filter is noiseless; the in-band filter loss is absorbed into the amplifier stage that follows, therefore the in-band gain is 1 and the out-of-band attenuation is L .
- 4) The out-of-band input noise N_{ino} is filtered by the anti-aliasing front-end bandpass filter ($N_{ino} = N_{\text{inp}}/L$ where L is the attenuation factor). The out-of-band is considered to be at all harmonics outside of the main $m = 0$ harmonic of the noise transfer function $H_m(f)$.
- 5) The device added noise is white, stationary, and unfiltered ($N_{ao} = N_{ap} = N_a$).
- 6) The switching is ideal, with zero rise and fall times. The switching devices have perfect ‘‘ON’’ and ‘‘OFF’’ states, and are themselves noiseless.

In the case of a time division multiplexer, the noise per multiplexed channel is analyzed first. In order to do this, the multiplexing portion of the circuit is divided into different stages as shown in Fig. 6. The first stage is the filter stage, followed by

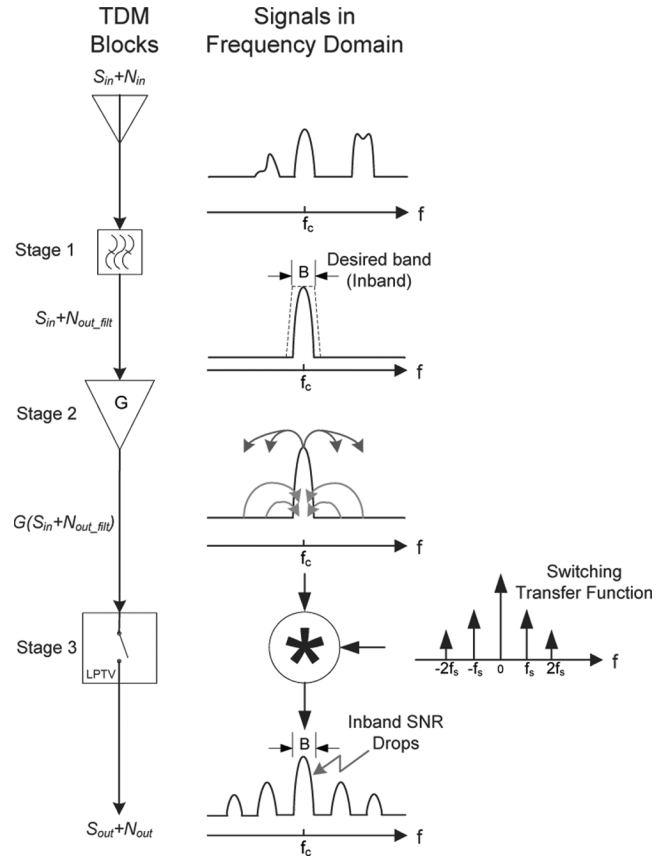


Fig. 6. TDM as an LPTV system.

the amplifier and then the switching stage which is actually responsible for the LPTV properties of the system.

The noise output from the amplifying stage is simply

$$N_{\text{out_amp}}(f) = GN_{\text{out_filt}}(f). \quad (20)$$

By using the relations developed in [23], the noise output of the LPTV stage may be written as

$$N_{\text{out,p}} = G \sum_{m=-\infty}^{\infty} |H_m(f_c)|^2 N_{\text{out_filt}}(f_c + mf_s) \quad (21)$$

where $H_m(f_c)$ is the noise transfer function at the RF carrier frequency, and is formally defined as

$$H_m(f_c) = \int_{-\infty}^{\infty} \left[\frac{1}{T} \int_0^T h(v+u, u) e^{j2\pi m f_s u} du \right] e^{-j2\pi f_c v} dv \quad (22)$$

where $h(v+u, u)$ is the impulse response of the LPTV system.

In this analysis under the assumptions previously stated, (22) simplifies to

$$H_m(f_c) = P_m \quad (23)$$

where P_m are the Fourier coefficients of the pulse train, defined in (10).

In a practical system, all the noise harmonics of equation will not have to be considered and only those within an effective

bandwidth B_{eff} around the RF carrier f_c will have to be evaluated. Equation (21) may be rewritten as for the practical case

$$N_{\text{outp}} = G \sum_{m=-\lfloor B_{\text{eff}}/2f_s \rfloor}^{\lfloor B_{\text{eff}}/2f_s \rfloor} |H_m(f_c)|^2 N_{\text{out_filt}}(f_c + mf_s). \quad (24)$$

In this analysis, however, the worst case scenario of all harmonics through to infinity are considered which allows the use of the following identity:

$$\begin{aligned} \sum_{m=-\infty}^{\infty} |H_m(f_c)|^2 &= \sum_{m=-\infty}^{\infty} P_m^2 \\ &= \sum_{m=-\infty}^{\infty} \left(\frac{\sin\left(\frac{m\pi}{N}\right)}{m\pi} \right)^2 = \frac{1}{N}. \end{aligned} \quad (25)$$

Rewriting (25) after pulling out the $m = 0$ term

$$\sum_{\substack{m=-\infty \\ m \neq 0}}^{\infty} |H_m(f_c)|^2 = \sum_{\substack{m=-\infty \\ m \neq 0}}^{\infty} \left(\frac{\sin\left(\frac{m\pi}{N}\right)}{m\pi} \right)^2 = \frac{1}{N} - \frac{1}{N^2}. \quad (26)$$

Using (21) and (26), the noise factor of a single TDM amplifier case is given by equation (27) at the bottom of the page.

The best and worst case noise factors may be obtained as

$$\begin{aligned} F_{TDM_amp} &= N \cdot F_{\text{amp}} \quad \text{if } L = 1 \text{ (worst case)} \\ F_{TDM_amp} &= N \cdot F_{\text{amp}} - (N - 1) \quad \text{if } L \rightarrow \infty \text{ (best case)}. \end{aligned} \quad (28)$$

Since the noise under consideration is for the front-end amplifier section, it follows from Friis' noise factor relationship that the system noise figure is impacted by the same factor as the amplifier noise figure. Thus from a single multiplex channel perspective, if no coherent signal combining process such as diversity or beamforming is exploited in the TDM system, the sensitivity of the receiver degrades by a maximum of $10 \log(N)$ dB. This degradation compared to the conventional receiver occurs if only the output from a single multiplex channel is processed at baseband. This is of relevance in the MIMO-SM case where individual antenna data streams can be expected to suffer an SNR, hence BER, degradation when compared to an equivalent continuous channel in a conventional multiantenna receiver. However based on the following capacity equation for MIMO systems

$$C = B_{ch} \min(M, N) \log_2(1 + \text{SNR}) \text{bps} \quad (29)$$

where B_{ch} is the wireless channel bandwidth, M the number of transmit antennas, and N the number of receive antennas, the capacity of the MIMO receiver is less dependent on degradation

of SNR due to the log relationship. The TDM approach still offers N independent receive channels with which the system capacity has a direct dependence.

The performance of the TDM wireless receiver is also placed in context by comparing its array noise factor with those of the more conventional single antenna receiver and coherent combining receivers. These are considered one at a time below. The available SNR at each antenna is assumed to be

$$\text{SNR}_{\text{in}} = \frac{S_{\text{in}}}{N_{\text{inp}}}. \quad (30)$$

1) Single Antenna Receiver:

$$F_{\text{single}} = \frac{\text{SNR}_{\text{in}}}{\text{SNR}_{\text{single}}} = 1 + \frac{N_a}{N_{\text{inp}}} = 1 + \frac{N_{ai}}{N_{\text{inp}}}. \quad (31)$$

In (31) and in the analysis that follows, N_a is assumed to be the overall device added noise in the system and G the overall system gain.

2) *Multiantenna Conventional (Non-TDM) Coherent Combining Receiver:* Since the noise is assumed to be uncorrelated, they will add in power, while the signals being coherent will add in amplitude after coherent combining. Therefore

$$F_{\text{conv_array}} = \frac{\text{SNR}_{\text{in}}}{\text{SNR}_{\text{conv_array}}} = \frac{1}{N} \left(1 + \frac{N_{ai}}{N_{\text{inp}}} \right) = \frac{1}{N} \cdot F_{\text{single}} \quad (32)$$

3) *Multiantenna TDM Coherent Combining Receiver:* Under the previously stated assumptions, with the switching takes place immediately following the amplifiers, the output array SNR is

$$\begin{aligned} \text{SNR}_{TDM_array} &= \\ &= \frac{(N \cdot \frac{1}{N} \sqrt{GS_{\text{in}}})^2}{N \left(\frac{G}{N^2} N_{\text{inp}} + \frac{1}{N^2} N_{ap} + G \left(\frac{1}{N} - \frac{1}{N^2} \right) N_{\text{ino}} + \left(\frac{1}{N} - \frac{1}{N^2} \right) N_{ao} \right)} \end{aligned} \quad (33)$$

$$\text{SNR}_{TDM_array} = \frac{GS_{\text{in}}}{G \left(\frac{1}{N} + \frac{1}{L} \left(1 - \frac{1}{N} \right) \right) N_{\text{inp}} + N_a} \quad (34)$$

$$\begin{aligned} \text{SNR}_{TDM_array} &= \text{SNR}_{\text{single}} = \frac{\text{SNR}_{\text{conv_array}}}{N}, \\ &\quad \text{if } L = 1 \text{ (worst case)}. \end{aligned} \quad (35)$$

and

$$\begin{aligned} F_{TDM_array} &= \frac{\text{SNR}_{\text{in}}}{\text{SNR}_{TDM_array}} \\ &= \left(\frac{1}{N} + \frac{1}{L} \left(1 - \frac{1}{N} \right) \right) + \frac{N_{ai}}{N_{\text{inp}}} \\ &= F_{\text{single}} - \left(1 - \frac{1}{N} \right) \left(1 - \frac{1}{L} \right) \end{aligned} \quad (36)$$

$$F_{TDM_array} = F_{\text{single}} = N \cdot F_{\text{conv_array}}, \quad \text{if } L = 1 \text{ (worst case)}$$

$$\begin{aligned} F_{TDM_amp} &= \frac{\left(\frac{S}{N} \right)_{\text{in}}}{\left(\frac{S}{N} \right)_{\text{out}}} = \frac{N^2 N_{\text{outp}}}{G N_{\text{inp}}} = \frac{N^2}{G} \left[\frac{\frac{G}{N^2} N_{\text{inp}} + \frac{1}{N^2} N_{ap} + G \left(\frac{1}{N} - \frac{1}{N^2} \right) N_{\text{ino}} + \left(\frac{1}{N} - \frac{1}{N^2} \right) N_{ao}}{N_{\text{inp}}} \right] \\ F_{TDM_amp} &= \left(1 + (N - 1) \frac{1}{L} \right) + N \frac{N_{ai}}{N_{\text{inp}}} = N \cdot F_{\text{amp}} - (N - 1) \left(1 - \frac{1}{L} \right). \end{aligned} \quad (27)$$

$$F_{TDM_array} = F_{single} - \left(1 - \frac{1}{N}\right), \quad \text{if } L \rightarrow \infty \text{ (best case),} \quad (37)$$

It may be summarized

$$SNR_{single} \leq SNR_{TDM_array} \leq SNR_{conv_array} \quad (38)$$

or equivalently

$$F_{conv_array} \leq F_{TDM_array} \leq F_{single}. \quad (39)$$

The conclusion from these results is that in the theoretical limit of infinite signal path bandwidth the difference in noise performance is *independent* of antenna channel sample rate and is only related to the number of multiplexed channels and the anti-aliasing bandpass filter characteristics. However in the real world, due to the availability of only finite signal path bandwidth, it follows from (24) and the transfer function coefficients as given by (23) and (10), that the noise aliasing is minimized with wider pulses and greater sample rates. Wider pulses and higher sampling rates have an inverse relationship, just as the need for wider pulses to minimize noise and narrower pulses to minimize inter-multiplexed-channel crosstalk have an inverse relationship.

III. TDM FRONT-END AMPLIFIER CIRCUIT

This TDM front-end amplifier stage was implemented as a fully differential version of the circuit described in [24] in a 0.18 μm SiGe BiCMOS process that required a 1.8 V supply voltage. Only the CMOS option was exercised in this design. The differential circuit was balanced with respect to the switching signals in order to limit switching clock feedthrough. The amplifier stage consisted of an array of differential LNA unit cells in a parallel arrangement so as to achieve RF current summation at the output. The input matching network was designed for 100 Ω differential impedance. This matching network can be optimized with noise/power matching techniques described in [25]–[27]. The differential 100 Ω at the combiner output was realized with a single L-C matching network. Bandwidth extending methods available in [28], [29] are appropriate for broadbanding this output. The matching networks were implemented with on-chip spiral inductors in series with off-chip bond wires, and a single external capacitor. The differential 100 Ω signals were converted to single ended 50 Ω impedances for measurement purposes using external $\sqrt{2} : 1$ balun transformers.

A. RF TDM Amplifier and CML Buffer

Each LNA unit cell shown in Fig. 8 was comprised of a differential LNA core, a differential current mode logic (CML) switch drive buffer and a current mirror network for biasing the amplifier and CML. The source coupled inductively degenerated LNA core was designed to be noise matched to a differential 100 Ω input while simultaneously providing at least 0 dBm IIP3 linearity for a 6 mA current consumption. The LNA core switches were driven by the differential control signals from the CML

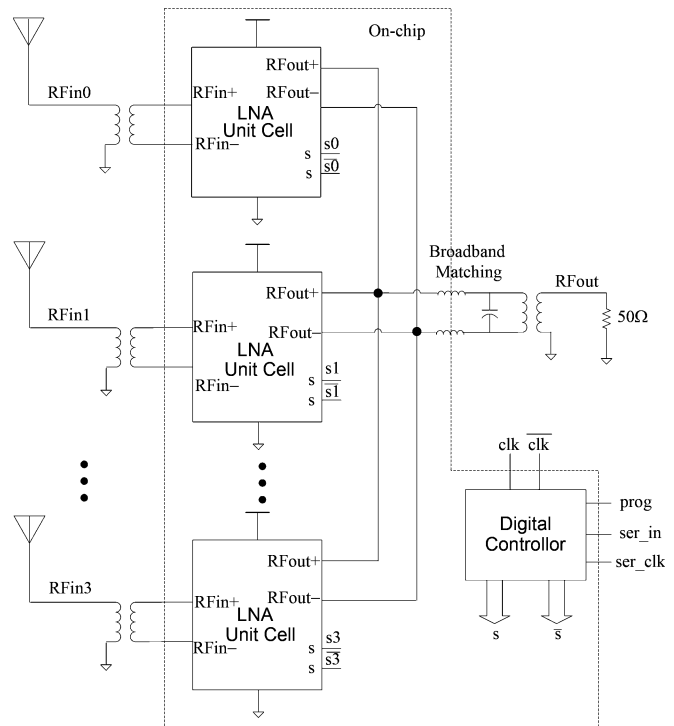


Fig. 7. TDM front-end amplifier stage.

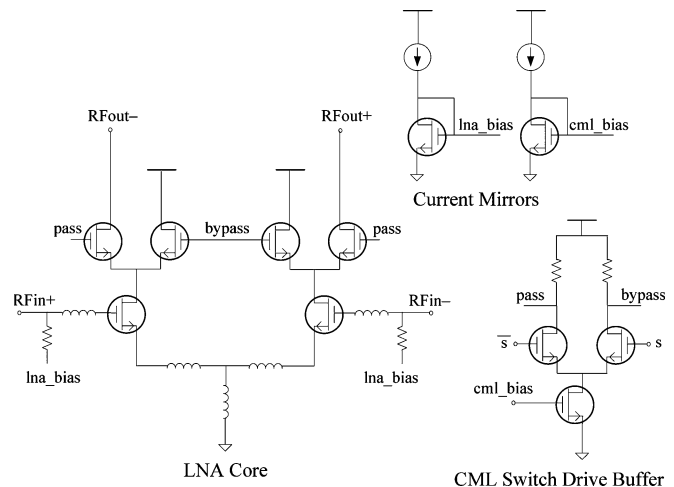


Fig. 8. Differential LNA unit cell.

buffer. A differential cascode style was chosen for the LNA core, with the cascode current steering pair diverting the amplified signal either to the output or to the supply when that multiplex signal path had to be disabled. The cascode circuit style contributes to the high isolation between the RF input and the combiner output while the differential current steering topology enabled fast switching with sharp transitions. An LNA core of this kind also helps maintain uniform loading on the antenna elements regardless of the on/off state of each channel.

The CML buffers used to drive the switching devices had an output swing of 225mV below the analog supply and consumed 750 μA of current from the same supply. The buffers' gate drives were provided by a digital controller.

B. Digital Controller

High speed hybrid latch flip-flops (HLFFs) were used to implement the digital controller. Each of the front-end amplifiers was assigned a register row that could hold a byte-length digital sequence. All these registers could be serially programmed as needed to operate the required amplifiers in the required order. The real advantage of this controller configuration is seen when measurements need to be made on a single amplifier with all other amplifiers effectively inactive.

A register row of length eight will permit only two or four amplifiers to be brought into TDM operation without wasting a time slot in a four amplifier array. The stored bit sequences could be scanned out at a much higher differential clock rate to control the switching in the amplifier section. The high speed differential clock was buffered by the differential clock input buffer that was based on a fully complementary self-bias design. In post-layout simulations with parasitics extracted, the controller operated correctly for clock rates till 2 GHz.

C. Chip Layout

Isolated triple-well structures were employed for all the nFET devices to decrease the effect of noise and spurious content on the circuit. The amplifiers were also arranged to minimize performance variations while sequentially switching from one to the other due to layout mismatches. All pads were provided with minimum recommended ESD protection.

Carefully partitioning of the RF and digital portions of the chip was done to minimize the impact of digital switching noise on the RF signals. The analog and digital supplies were separated and allotted multiple pads in order to minimize switching noise. Similar precautions were taken for the ground by providing for separate analog and digital grounds spread over multiple pads to reduce the ground bounce. Decoupling capacitors were incorporated both on and off-chip to reduce noise on the supplies and biases.

The chip layout shown in Fig. 9 was completed with the intention of testing it by wirebonding it directly to a two-layer RF circuit board. The circuit area, ignoring the bondpads was $2460 \mu\text{m} \times 1310 \mu\text{m}$.

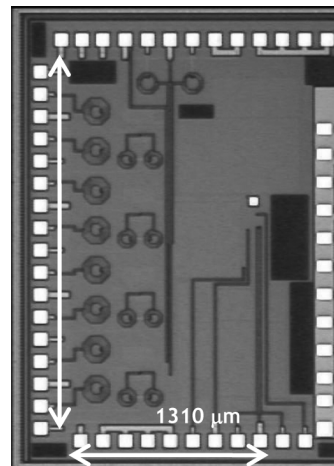


Fig. 9. Circuit die photograph of the $0.18 \mu\text{m}$ design in CMOS.

TABLE I
STATIC AMPLIFIER CHANNEL RESPONSES (Port1 = RFin3 AND
Port2 = RFout) AT 2.4 GHz

Parameter	Channel On	Channel Off
S11 (dB)	-12.8	-11.4
S12 (dB)	-36.6	-45.4
S21 (dB)	7.4	-46.3
S22 (dB)	-13.7	-14.6
NF (dB)	2.6	-
IIP3 (dBm)	0.3	-
Current/CML Buffer (mA)		0.75
Current/LNA Core (mA)		6
Supply (V)		1.8

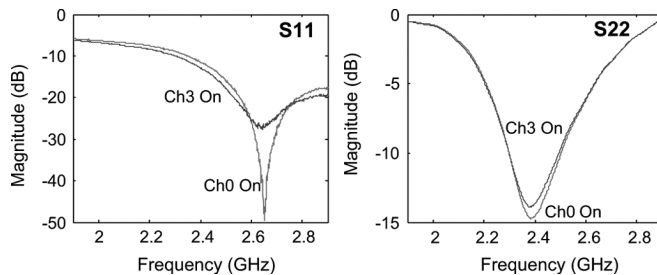


Fig. 10. Input and output matching (Port1 = RFin3 and Port2 = RFout).

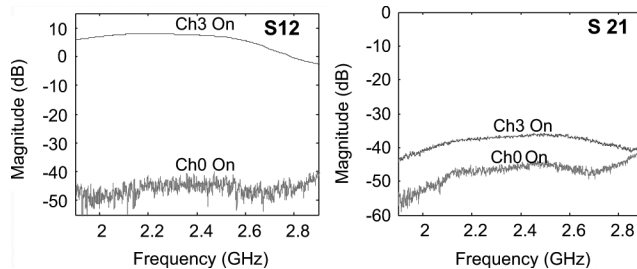


Fig. 11. Forward and reverse gain (Port1 = RFin3 and Port2 = RFout).

IV. RESULTS

A. Static Amplifier Response

The results of the S -parameter measurements done on a single nonswitching amplifier channel termed a “static amplifier” are shown in Table I. The matching and gain curves are shown in Figs. 10 and 11. It is observed that the switched LNA’s ON-OFF isolation at 2.4 GHz is 53.8 dB. The forward gain S21 peaks at 8.0 dB at 2.23 GHz. The 3 dB bandwidth with reference to this peak gain point is 819.7 MHz.

B. Noise Figure Measurements

The noise figure measurements were done for a sample rate f_s of 40 MHz per channel selected to ensure that device gain is linear over the measurement span set equal to f_s . A center frequency of 2.41 GHz was chosen for this sample rate based on

(5). The Agilent PSA E4440A spectrum analyzer along with an Agilent 346A noise source was used for the noise figure measurements. The raw spectral data was analyzed in Matlab using the modified Y -factor method described in the Appendix to evaluate the correct noise measures for a TDM wireless receiver.

TABLE II
SUMMARY OF NOISE MEASUREMENTS AT 2.41 GHz

Characteristic	Mean Performance (Over 40 MHz Span)	
Static Amplifier Available Gain (dB)	7.1	
Static Amplifier Noise Figure (dB)	2.6	
	Number of Multiplexed Elements	
	$N = 2$	$N = 4$
TDM Amplifier Noise Gain (dB)	3.9	0.4
$\Delta 1$ Noise Gain (dB)	-3.2	-6.6
TDM Amplifier Noise Figure (dB)	4.8	7.9
$\Delta 1$ Noise Figure (dB)	2.1	5.3
Available TDM Amp Array NF (dB)	1.8	1.9
$\Delta 2$ Noise Figure (dB)	-0.9	-0.7

$\Delta 1$: [TDM Amp – Static Amp]
 $\Delta 2$: [Available TDM Amp Array – Static Amp]

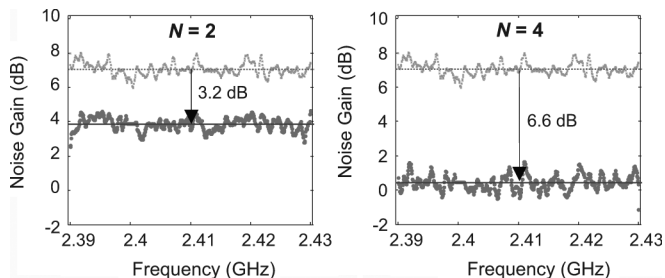


Fig. 12. Noise gain per antenna channel (... Static Amp,—TDM Amp).

The noise characteristics of the front-end were evaluated for two TDM cases, the multiplexing of $N = 2$ and $N = 4$ channels. The results presented are indeed the worst case for the designed circuit since they do not involve any additional bandpass anti-alias filtering other than those inherently provided by the circuit’s own matching networks. These results were compared with that of a reference static amplifier. The noisy raw data was averaged over the measurement span in order to obtain the results are summarized in Table II. The RSS noise figure measurement uncertainty was calculated to be 0.26 dB.

In Fig. 12, the ratio of output noise attributed to the input noise alone to input noise defined as the noise gain (more details in Appendix) is shown for the two cases considered. We observe that the fall in noise gain in the two cases is slightly more than the theoretical minimum of $10 \log(N)$. One reason for this is the small degree of input noise filtering provided by the matching network at the input. Additional filtering would result in a lowering in noise gain as determined by the previously presented theory and the relations in the Appendix .

The worst case SSB noise figure per amplifier channel is presented in Fig. 13. In both cases they are below the maximum $10 \log(N)$ increase above that of a static amplifier.

A better appreciation of the effect of individual channel noise figure results may be obtained by determining the overall array noise figures shown in Fig. 14. This involves scaling down the single channel noise figure by a factor of N based on the previously developed theory. Since the complete receiver has not been implemented in this work, only the “available” noise figure

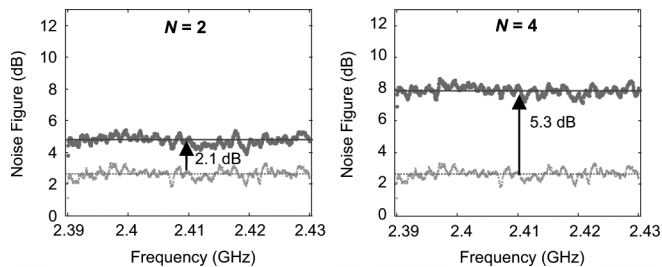


Fig. 13. Noise figure per antenna channel [SSB] (... Static Amp,—TDM Amp).

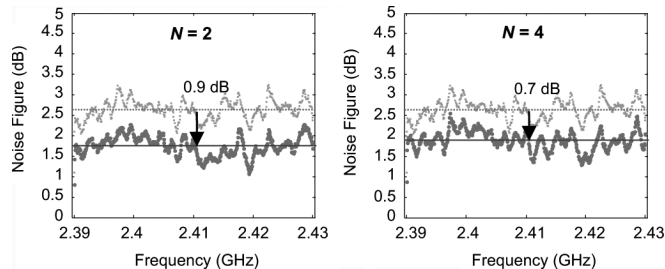


Fig. 14. Available array noise figure [SSB] (... Static Amp,—TDM Amp).

based on the amplifier section can be calculated from the measured data. This is still a relevant measure of performance of the TDM-based receiver because of its location in the receiver chain closely following the antenna, hence having a large influence on the overall noise figure.

The noise figure of the TDM amplifiers was observed to improve with higher sample rates f_s as can be expected from (24). The exact nature of the dependence is yet to be quantified.

A final comparison of the available TDM array noise figure with that of the single amplifier shows that it is better than that of the static amplifier for the cases considered. This is in agreement with the overall theory presented earlier, and inequality (39) specifically.

It must also be emphasized that the presented *results are all worst case* since an explicit alias reject filter is not included before the switching amplifiers. With the presence of this filtering the noise figures of the TDM amplifier and array will be appreciably better.

C. Linearity Measurement

The same multiplex rate and bias conditions as the noise measurements were retained for the linearity measurements. The in-band linearity of the amplifier channels as given by the third-order Intercept point is unaffected by the TDM operation as is seen in Fig. 15. This result is expected as the TDM switching is done at rates that are high enough not to adversely affect either the inband spectrum or the wireless channel spectrum, which is a subset of the inband spectrum.

With the gain flat over the inband frequencies, the effect of the multiplex operation is to attenuate the desired signal component and the IM3 component by the same factor. This causes the amplifiers power output curves to be displaced downwards without affecting the IIP3 of that channel.

The combined effect of the increased noise figure and unchanged linearity is a decrease in dynamic range per multiplex

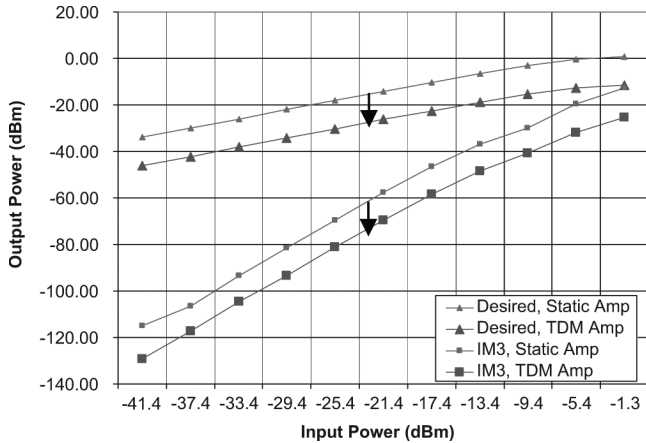


Fig. 15. Linearity measurement plots for a single amplifier channel.

TABLE III
PERFORMANCE COMPARISON OF DIFFERENT RECEIVER TYPES

Comparison Metric	Single Antenna	Multi-Antenna TDM	Multi-Antenna Conventional
Available Array NF (dB)	2.6	1.9 [#]	-3.4
Available Array Signal Gain (dB)	7.1	7.1	19.1
Net Array Power Estimate (mW)	10.8 + $P_{post-amp}$	48.6 + $P_{post-amp}$	43.2 + $4.P_{post-amp}$
Linearity as IIP3/antenna (dBm)	0.3	0.3	0.3
Array Dynamic Range	Low	Mid	High
Throughput enhancement possible by Spatial Multiplexing	None (1x)	4x	4x
Interference Cancellation	No	Yes	Yes

[#] Without alias reject filtering (worst case)

channel by the same degree as the noise figure. By the same token, the combined array dynamic range would be better than that of a single antenna receiver but worse than that of a conventional non-TDM array.

D. Performance Comparison

A summarized view of the implemented four-antenna TDM receiver front-end performance vis-à-vis the reference single antenna and conventional multiantenna receiver front-ends is shown in Table III. In order to appreciate the power utilization implications of the different approaches, the post-amplifier stages of the receiver are also factored in, although this portion of the receiver is not realized in this work. It is assumed that these stages consume $P_{post-amp}$ mW in a single antenna system.

It can be inferred from this table that the multiantenna TDM receiver provides a level of performance that is above that of a single antenna system but below that of a full-fledged conventional multiantenna system. The TDM based multiantenna receiver offers many of the advantages of the conventional multiantenna receiver, but at lower power and area costs.

V. CONCLUSION

A detailed look at the prospects of time division multiplexing as a solution to the hardware duplication problem in multi-antenna receivers was presented. An analysis based on first principles of bandpass sampling and TDM theory is offered. A hardware solution to the problem of crosstalk between multiplex channels with channel filtering is proposed. Closed form relations for noise figure are developed that are useful for quick figure of merit evaluations of the TDM architecture. An important insight gained from the theoretical treatment is that in general it can be expected that the noise figure (and array output SNR) of a coherent combining TDM receiver is better than that of a single antenna receiver but worse than that of a conventional multiantenna array. The noise figure relations can easily be generalized to accommodate the additional filtering and switching nonidealities that would occur in practice.

A fully differential front-end consisting of a four 2.4 GHz amplifier array is fabricated as a CMOS circuit in a 0.18 μ m process. This front-end circuit is used to verify the presented theory. The results obtained from the noise measurements validate the simple model of the TDM front-end and its usefulness in understanding the performance. Linearity measurements provided finally help address the dynamic range concerns of this receiver architecture.

APPENDIX

RELATIVE MEASUREMENT TECHNIQUE FOR NOISE FIGURE MEASUREMENT OF TDM FRONT-END

The Y-factor method is the most common noise figure measurement technique used in practice [30]. Since the TDM front-end has frequency conversion effects and multiple side bands are inherent in its working, the Y-Factor method has to be modified to correctly characterize its noise figure.

The overall noise added by the switching (frequency translating) device is a combination of frequency translated source noise and the noise due to the device alone

$$N_{aoverall}(T_c, T_s) = (G_{ASB} - G_s)kT_sB + \hat{N}_a(T_c) \quad (A1)$$

where $\hat{N}_a(T_c)$ is the noise due to the device alone at physical temperature T_c , T_s is the source noise temperature, G_s is the desired signal conversion gain (of the zeroth harmonic in the TDM case) and G_{ASB} is the noise gain defined as the ratio of the net output noise due to the input noise alone to the input noise at the same frequency. By definition, G_{ASB} is an all side band measure. In nonfrequency translating devices such as regular amplifiers $G_{ASB} = G_s$.

The generally calculated noise factor is actually the all side band (ASB) noise factor F_{ASB} expressed as

$$\begin{aligned} F_{ASB} &= \frac{N_{out}}{G_{ASB}kT_0B} \\ &= \frac{G_s kT_0B + N_{aoverall}(T_c, T_0)}{G_{ASB}kT_0B} \\ &= \frac{G_{ASB}kT_0B + \hat{N}_a(T_c)}{G_{ASB}kT_0B} \end{aligned} \quad (A2)$$

from which

$$\hat{N}_a(T_c) = G_{ASB}kT_0B(F_{ASB} - 1). \quad (A3)$$

The relevant measure of noise performance in the TDM context is the single sideband (SSB) noise factor F_{SSB} as defined by Haus *et al.*[31] and given by

$$\begin{aligned} F_{SSB} &= \frac{N_{out}}{G_s k T_0 B} = 1 + \frac{N_{aoverall}(T_c, T_0)}{G_s k T_0 B} \\ &= \frac{G_{ASB}kT_0B + \hat{N}_a(T_c)}{G_s k T_0 B}. \end{aligned} \quad (A4)$$

Substituting for $\hat{N}_a(T_c)$ in (A7) from (A6) above and simplifying we have

$$F_{SSB} = \frac{G_{ASB}}{G_s} F_{ASB}. \quad (A5)$$

G_{ASB} is determined as part of the standard Y -factor noise measurement technique. In addition, G_s will have to be measured too to determine F_{SSB} of the TDM wireless receiver.

In relation to the previous analysis of a single TDM amplifier channel in Section II-C, it is readily found that

$$\begin{aligned} G_{ASB} &= \frac{G}{N} \left(\frac{1}{N} + \frac{1}{L} \left(1 - \frac{1}{N} \right) \right) \\ G_s &= \frac{G}{N^2} \\ \hat{N}_a(T_c) &= \frac{N_a}{N}. \end{aligned} \quad (A6)$$

As it is not possible to accurately determine the added noise $\hat{N}_{a-TDM_amp}(T_0)$, hence the F_{ASB} , of a single TDM amplifier channel directly, an indirect relative measurement technique is adopted to obtain this value. This approach involves the measurement of net output noise during TDM operation after terminating all the inputs to the TDM array with the same cold noise terminations. Assuming that the N TDM channels are all identical, we may then determine the ratio R of the output noise from the TDM array to the output noise from a single static amplifier as

$$\begin{aligned} R &= \frac{N_{out-TDM_array}}{N_{out_amp}} \\ &= \frac{N \left(G_{ASB}kT_cB + \hat{N}_{a-TDM_amp}(T_c) \right)}{GkT_cB + \hat{N}_{a_amp}(T_c)} \\ &= \frac{N \left(G_{ASB}kT_cB + (F_{ASB-TDM_amp} - 1) G_{ASB}kT_0B \right)}{GkT_cB + (F_{amp} - 1)GkT_0B} \\ &= \frac{NG_{ASB} \left(T_c + (F_{ASB-TDM_amp} - 1) T_0 \right)}{G \left(T_c + (F_{amp} - 1) T_0 \right)}. \end{aligned} \quad (A7)$$

Simplifying (A7) further we obtain

$$\begin{aligned} F_{ASB-TDM_amp} &= \frac{RG}{NG_{ASB}} \left((F_{amp} - 1) + \frac{T_c}{T_0} \right) + \left(1 - \frac{T_c}{T_0} \right). \end{aligned} \quad (A8)$$

All the factors on the right side of (A8) being either measured or known beforehand, we can determine F_{ASB} of the TDM amplifier. The single sideband noise figure F_{SSB} of this TDM amplifier may then be computed using (A5).

ACKNOWLEDGMENT

The authors would like to thank Dr. S. Lipa for assistance with wirebonding the chip onto the test board.

REFERENCES

- [1] J. H. Winters, "Smart antennas for wireless systems," *IEEE Personal Commun.*, vol. 5, pp. 23–27, 1998.
- [2] J. Winters, J. Salz, and R. Gitlin, "The impact of antenna diversity on the capacity of wireless communication systems," *IEEE Trans. Commun.*, vol. 42, no. 2/3/4, pp. 1740–1751, Feb./Mar./Apr. 1994.
- [3] L. C. Godara, "Applications of antenna arrays to mobile communications. I. performance improvement, feasibility, and system considerations," *Proc. IEEE*, vol. 85, no. 7, pp. 1031–1060, Jul. 1997.
- [4] L. C. Godara, "Application of antenna arrays to mobile communications. II. Beam-forming and direction-of-arrival considerations," *Proc. IEEE*, vol. 85, no. 8, pp. 1195–1245, Aug. 1997.
- [5] A. J. Paulraj, D. A. Gore, R. U. Nabar, and H. Bolcskei, "An overview of MIMO communications—A key to gigabit wireless," *Proc. IEEE*, vol. 92, no. 2, pp. 198–218, Feb. 2004.
- [6] R. G. Vaughan, N. L. Scott, and D. R. White, "The theory of bandpass sampling," *IEEE Trans. Signal Process.*, vol. 39, no. 9, pp. 1973–1984, Sep. 1991.
- [7] W. R. Bennett, "Time division multiplex systems," *Bell Syst. Tech. J.*, vol. 20, pp. 199–221, Apr. 1941.
- [8] H. Luke, "The origins of the sampling theorem," *IEEE Commun. Mag.*, vol. 37, no. 4, pp. 106–108, Apr. 1999.
- [9] H. H. Beverage and H. O. Peterson, "Diversity receiving system of R. C. A. communications, Inc., for radiotelegraphy," in *Proc. Inst. Radio Eng.*, Apr. 1931, vol. 19, pp. 531–561.
- [10] M. Murase, Y. Tanaka, and H. Arai, "Propagation and antenna measurements using antenna switching and random field measurements," *IEEE Trans. Veh. Technol.*, vol. 43, no. 3, pp. 537–541, Aug. 1994.
- [11] F. Adach, T. Hattori, K. Hirade, and T. Kamata, "A periodic switching diversity technique for a digital FM land mobile radio," *IEEE Trans. Veh. Technol.*, vol. 27, no. 4, pp. 211–219, Nov. 1978.
- [12] L. Saporta and K. Steiglitz, "Crosstalk in time division multiplex systems," *IEEE Trans. Commun. Syst.*, vol. 11, no. 2, pp. 250–253, Jun. 1963.
- [13] D. S. Goshi, Y. Wang, and T. Itoh, "A compact digital beamforming SMILE array for mobile communications," *IEEE Trans. Microw. Theory Tech.*, vol. 52, no. 12, pp. 2732–2738, Dec. 2004.
- [14] J. D. Fredrick, Y. Wang, and T. Itoh, "Smart antennas based on spatial multiplexing of local elements (SMILE) for mutual coupling reduction," *IEEE Trans. Ant. Propag.*, vol. 52, no. 1, pp. 106–114, Jan. 2004.
- [15] O. Degani, M. Ruberto, E. Cohen, Y. Eilat, B. Jann, F. Cossoy, N. Telzhensky, T. Maimon, G. Normatov, R. Banin, O. Ashkenazi, A. Ben Bassat, S. Zaguri, G. Hara, M. Zajac, E. Shaviv, S. Wail, A. Fridman, R. Lin, and S. Gross, "A 1×2 MIMO multi-band CMOS transceiver with an integrated front-end in 90 nm CNOS for 802.11a/g/n WLAN applications," in *ISSCC Dig. Tech. Papers*, Feb. 2008, pp. 356–357.
- [16] A. Behzad, K. Carter, E. Chien, S. Wu, M. Pan, C. Lee, T. Li, J. Leete, S. Au, M. Kappes, Z. Zhou, D. Ojo, L. Zhang, A. Zolfaghari, J. Castanada, H. Darabi, B. Yeung, R. Rofougaran, M. Rofougaran, J. Trachewsky, T. Moorti, R. Gaikwad, A. Bagchi, J. Rael, and B. Marhoiev, "A fully integrated MIMO multi-band direct-conversion CMOS transceiver for WLAN applications (802.11n)," in *ISSCC Dig. Tech. Papers*, 2007, pp. 560–622.
- [17] A. Safarian, L. Zhou, and P. Heydari, "CMOS distributed active power combiners and splitters for multi-antenna UWB beamforming transceivers," *IEEE J. Solid-State Circuits*, vol. 42, no. 7, pp. 1481–1491, Jul. 2007.
- [18] X. Guan, H. Hashemi, and A. Hajimiri, "A fully integrated 24-GHz eight-element phased-array receiver in silicon," *IEEE J. Solid-State Circuits*, vol. 39, no. 12, pp. 2311–2320, Dec. 2004.

- [19] H. Rafati and B. Razavi, "A receiver architecture for dual-antenna systems," *IEEE J. Solid-State Circuits*, vol. 42, no. 6, pp. 1291–1299, Jun. 2007.
- [20] F. Tzeng, A. Jahanaian, and P. Heydari, "A CMOS code-modulated path-sharing multi-antenna receiver front-end for spatial multiplexing, spatial diversity and beamforming," in *Proc. IEEE RFIC Symp.*, Jun. 2008, pp. 335–338.
- [21] K. Muhammad, R. Staszewski, and D. Leipold, "Digital RF processing: Toward low-cost reconfigurable radios," *IEEE Commun. Mag.*, vol. 43, no. 8, pp. 105–113, Aug. 2005.
- [22] A. Zanchi and C. Samori, "Analysis and characterization of the effects of clock jitter in A/D converters for subsampling," *IEEE Trans. Circuits Syst. I, Reg. Papers*, vol. 55, no. 2, pp. 522–534, Mar. 2008.
- [23] C. D. Hull and R. G. Meyer, "A systematic approach to the analysis of noise in mixers," *IEEE Trans. Circuits Syst. I, Reg. Papers*, vol. 40, no. 12, pp. 909–919, Dec. 1993.
- [24] G. Krishnamurthy and K. G. Gard, "Integrated time division multiplexing front-end circuit for multi-antenna RF receivers," in *Proc. IEEE RFIC Symp.*, Jun. 2008, pp. 351–354.
- [25] S. Asgaran, M. J. Deen, and C.-H. Chen, "Design of the input matching network of RF CMOS LNAs for low-power operation," *IEEE Trans. Circuits Syst. I, Reg. Papers*, vol. 54, no. 3, pp. 544–554, Mar. 2007.
- [26] L. Belostotski and J. W. Haslett, "Noise figure optimization of inductively degenerated CMOS LNAs with integrated gate inductors," *IEEE Trans. Circuits Syst. I, Reg. Papers*, vol. 53, no. 7, pp. 1409–1422, Jul. 2006.
- [27] G. Banerjee, K. Soumyanath, and D. J. Allstot, "Desensitized CMOS low-noise amplifiers," *IEEE Trans. Circuits Syst. I, Reg. Papers*, vol. 55, no. 3, pp. 752–765, Apr. 2008.
- [28] J. S. Walling, S. Shekhar, and D. J. Allstot, "Wideband CMOS amplifier design: Time-domain considerations," *IEEE Trans. Circuits Syst. I, Reg. Papers*, vol. 55, no. 7, pp. 1781–1793, Aug. 2008.
- [29] Y.-J. E. Chen and Y.-I. Huang, "Development of integrated broad-band CMOS low-noise amplifiers," *IEEE Trans. Circuits Syst. I, Reg. Papers*, vol. 54, no. 10, pp. 2120–2127, Oct. 2007.
- [30] Agilent, Santa Clara, CA, "Noise figure measurement accuracy—The Y-factor method," Literature Number 5952-3706E, Appl. Note 57-2, 2001.
- [31] H. A. Haus, R. Adler, R. S. Engelbrecht, S. W. Harrison, M. T. Lehenbaum, and W. W. Mumford, "Description of the noise performance of amplifiers and receiving systems," *Proc. IEEE*, vol. 51, no. 3, pp. 436–442, Mar. 1963.



Gautham Krishnamurthy (S'08) received the Bachelor's degree in electronics and communication engineering from R. V. College of Engineering, Bangalore, India, in 2002 and the M.S. degree in electrical engineering from North Carolina State University, Raleigh, in 2005, where he is currently working towards the Ph.D. degree in the area of efficient front-end circuits for multiple antenna receivers.

From 2002 to 2003, he worked with the Electronics and Radar Development Establishment, Bangalore, India, developing hardware and systems solutions for radar signal processing applications. His research interests include analog, RF and mixed-signal integrated circuits for communications, and signal processing applications.



Kevin G. Gard (S'92–M'95) received the B.S. and M.S. degrees in electrical engineering from North Carolina State University, Raleigh, in 1994 and 1995, respectively, and the Ph.D. degree in electrical engineering from the University of California at San Diego, La Jolla, in 2003.

He is currently a Hardware Design Engineer with Ericsson Mobile Platforms, where he designs CMOS front-end circuits for GSM, EDGE, and WCDMA transceivers. He is an Adjunct Professor with the Electrical and Computer Engineering (ECE)

Department, North Carolina State University (NCSU). From 2004 to 2008, he was the William J. Pratt Assistant Professor with the Electrical and Computer Engineering Department, NCSU. From 1996 to 2003, he was with Qualcomm Inc., San Diego, CA, where he was a Staff Engineer and Manager responsible for the design and development of RF integrated circuits (RFICs) for code-division multiple-access (CDMA) wireless products. His research interests include the areas of novel integrated circuit solutions for wireless transceivers and analysis of nonlinear microwave circuits with digitally modulated signals. He has authored or coauthored over 60 papers related to RF/analog integrated circuit design and analysis of nonlinear circuits. He is coinventor on three US and two European patents.

Dr. Gard was a member of the IEEE Microwave Theory and Techniques Society (IEEE MTT-S) and IEEE Solid-State Circuits Society. He is a member of Eta Kappa Nu and Tau Beta Pi. In 2007, He was secretary of the IEEE MTT-S Administrative Committee (AdCom) in 2007.